

# Dielectrics Newsletter

Scientific newsletter for dielectric spectroscopy

Issue december 2006

A. Serghei, F. Kremer

## Broadband Dielectric Spectroscopy on Ultra-Thin Films Having One Free Interface

Based on its unique ability to measure molecular fluctuations of polar moieties over a broad frequency and temperature range, Broadband Dielectric Spectroscopy (BDS) has proven in numerous recent studies its strengths in understanding the mechanisms of the confinement-effects in thin polymer films [1-5]. This technique has nevertheless a certain limitation: the standard procedure for the sample preparation [6] allows only measurements on thin films confined between two solid electrodes. Here we present a novel experimental approach which circumvents this drawback and enables one to carry

out dielectric measurements on ultra-thin organic layers having one *free* (upper) interface. A multitude of possible applications arise: ultra-thin liquid layers, thin layers of grafted polymers, liquid crystals and biomolecules, monolayers or perhaps even dielectric studies on single

(isolated) polymer chains.

The novel preparation procedure is schematically illustrated in fig. 1. Ultra-flat and highly conductive silicon wafers are used as electrodes. The root-mean square roughness of their surfaces is typically smaller than 0.5 nm on micrometric domains and their resistivity is below  $5 \cdot 10^{-3}$  Ohm cm. The wafers (0.3 mm thick) are initially covered by a protective layer of photoresist with a thickness of about  $\sim 700$  nm. They are cleaved along their crystallographic axes in small rectangular pieces of  $\sim 10$  mm  $\times$  5 mm and cleaned in an ultrasound bath of acetone (to remove the photoresist layer) and dichloromethane (to remove any particles from their surfaces). After this, a thin polymer layer is spin-coated onto one silicon wafer. On the surface of a second wafer a small amount of silica colloids (1  $\mu$ m diameter) is randomly spread from a water solution. The wafer with the sample and that with the colloids are brought in contact and slightly pressed against each other through a spring. The latter assures an optimal mechanical and electrical contact with the standard dielectric cell. At the same time it avoids breaking the rigid silica colloids and allows measurements in a broad temperature range. The silica particles act as spacers and keep the two electrodes separated at an interval equal to the their diameter. The film thickness is typically much smaller than the height of the spacers, thus, the samples are measured in a geometry having a *free* upper interface. This novel experimental approach is described in detail in ref. [7]. The

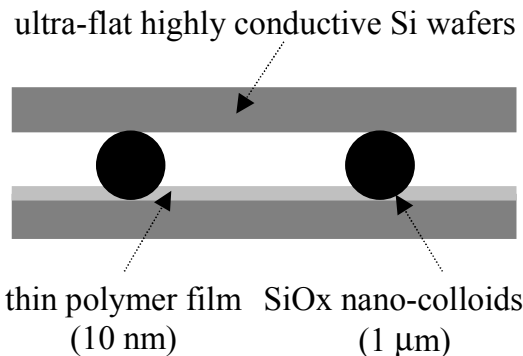


Fig. 1. Schematic representation of the preparation procedure.

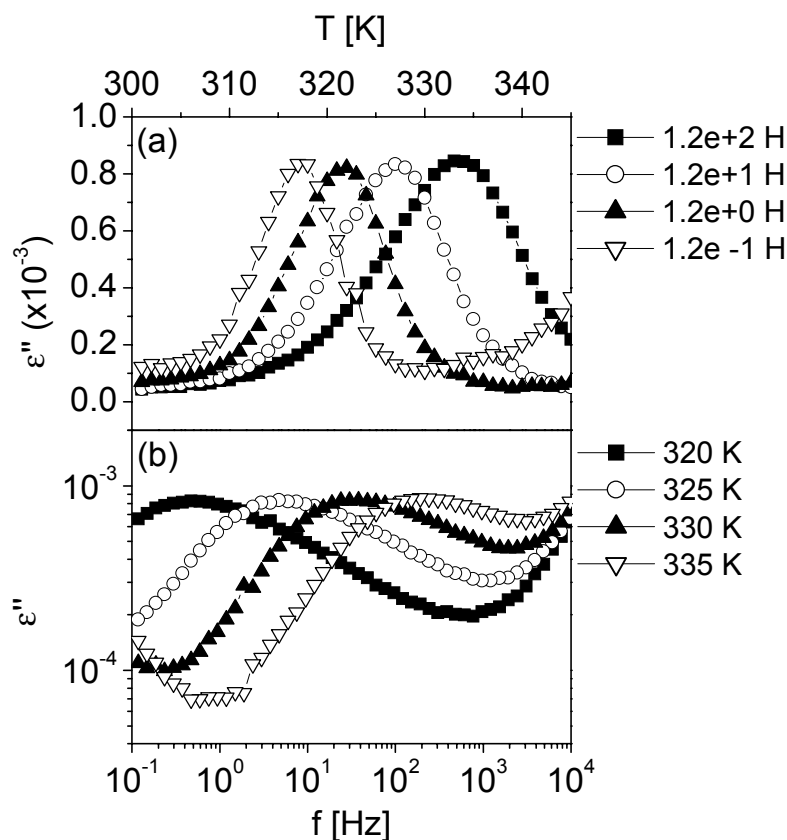


Fig. 2. (a) dielectric loss vs. temperature at different frequencies, as indicated, showing the dynamic glass transition of a thin film of polyvinylacetate having a thickness of 9 nm and the upper interface free; (b) the same experimental data plotted in spectra of dielectric loss vs. frequency at different temperatures.

relative area occupied by the spacers is optimized by diluting the colloidal suspension. At a concentration of ~0.5 mg/ml, typically 1.8% of the surface is occupied by the colloids.

Prior to dielectric measurements, the samples are annealed several hours in a pure nitrogen atmosphere (in the cryostat of the dielectric spectrometer) at temperatures well-above the glass transition. Immediately after annealing, the samples are measured without exposing them to ambient air again. The dielectric investigations are performed using a High Resolution Alpha Analyzer assisted by an Quatro temperature controller (Novocontrol GmbH).

Dielectric measurements using this novel preparation procedure are presented in fig. 2, for a thin film of polyvinylacetate having a thickness of 9 nm and a free upper interface. The peaks observed in the spectra of dielectric loss vs. temperature at different frequencies (fig. 2a) and dielectric loss vs. frequency at different temperatures (fig. 2b) represent the alpha relaxation process of polyvinylacetate – the dynamic glass transition of the investigated polymer. The sensitivity of this novel experimental approach can be significantly improved by reducing the height of the spacers, either by decreasing the diameter of the colloids or by employing nano-structures as nano-spacers. Both these alternatives were recently proven feasible [8]. This opens a manifold of completely new possibilities for the application of Broadband Dielectric Spectroscopy to investigate the molecular dynamics taking place on a nanometric length scale: ultra-thin liquid layers, organic monolayers, thin films of liquid crystals, grafted polymers and bio-molecules and may allow also for the extension of BDS to studies on single (macro)molecules.

**References**

[1] K. Fukao and Y. Miyamoto, Phys. Rev. E **61**, 1743 (2000).  
 [2] V. Lupascu et al., Thermochemica Acta **432**, 222 (2005).  
 [3] K. Fukao, Y. Miyamoto, Phys. Rev. E **64**, 011803 (2001).  
 [4] A. Serghei, M. Tress, and F. Kremer, Macromolecules, in press (2006).  
 [5] A. Serghei et al., J. Polym. Sci. B **44**, 3006 (2006).

[6] A. Serghei, and F. Kremer, Progress Colloid Polym. Sci. **132**, 33 (2006).

[7] A. Serghei, and F. Kremer, Rev. Sci. Instrum., in press (2006).

[8] A. Serghei, „*Confinement-effects on the molecular dynamics in thin polymer films*“, Ph.D. Thesis, Leipzig (2005).

Dr. A. Serghei and Prof. F. Kremer  
 Institute for experimental physics I,  
 University of Leipzig,  
 04103 Leipzig, Germany

**Appendix**

We analyse in the following in detail the complex dielectric function of a sample consisting in two layers, as illustrated in fig. 3: a thin organic film having a complex impedance  $Z_F^*$ , a thickness  $d_F$  and a complex permittivity  $\epsilon_F^*$  and a layer of air characterized by  $Z_A^*$ ,  $d_A$  and  $\epsilon_A^* = 1$ . The total impedance of the sample measured in the experiment is  $Z_M^* = Z_A^* + Z_F^*$ . Taking into account that

$\epsilon^* = \frac{-i}{\omega Z^* C_0}$ , where  $C_0$  represents the capacity of the empty sample capacitor, the previous relation leads to:  $\frac{D}{\epsilon_M^*} = d_A + \frac{d_F}{\epsilon_F^*}$ , where  $\epsilon_M^*$  is the measured complex permittivity.

Separating the real and the imaginary part in the latter equation gives:

$$(1) \quad \frac{D\epsilon'_M}{(\epsilon'_M)^2 + (\epsilon''_M)^2} - d_A = d_F \frac{\epsilon'_F}{(\epsilon'_F)^2 + (\epsilon''_F)^2} \quad \text{and}$$

$$(2) \quad \frac{D\epsilon''_M}{(\epsilon'_M)^2 + (\epsilon''_M)^2} = d_F \frac{\epsilon''_F}{(\epsilon'_F)^2 + (\epsilon''_F)^2}$$

Dividing the last two equations leads to:

$$(3) \quad \epsilon'_F = \epsilon''_F \frac{D\epsilon'_M - d_A [(\epsilon'_M)^2 + (\epsilon''_M)^2]}{D\epsilon''_M}$$

Introducing eq. (3) in eq. (1) gives:

$$\epsilon''_F = \epsilon''_M \frac{d_F}{D} \frac{(\epsilon'_M)^2 + (\epsilon''_M)^2}{\left[ \epsilon'_M - \frac{D-d_F}{D} [(\epsilon'_M)^2 + (\epsilon''_M)^2] \right]^2 + (\epsilon''_M)^2}$$

$$\epsilon'_F = \left[ (\epsilon'_M)^2 + (\epsilon''_M)^2 \right] \frac{d_F}{D} \frac{\epsilon'_M - \frac{D-d_F}{D} [(\epsilon'_M)^2 + (\epsilon''_M)^2]}{\left[ \epsilon'_M - \frac{D-d_F}{D} [(\epsilon'_M)^2 + (\epsilon''_M)^2] \right]^2 + (\epsilon''_M)^2}$$

These equations determine the absolute values of  $\epsilon'_F$  and  $\epsilon''_F$  as a function of the measured dielectric permittivity, film thickness  $d_F$  and diameter of the silica spacers  $D$ . In order to assess the dielectric data obtained in real experiments, one has to consider additionally the non-negligible contribution of the silicon electrodes to the measured impedance. For the sake of simplicity, this contribution has been neglected in the present calculations.

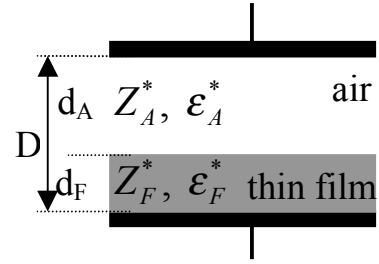


Fig. 3: scheme illustrating a sample capacitor consisting of two different layers.

S. Lerner, P. Ben Ishai, Y. Feldman

## High Frequency Time Domain Measurements of High Permittivity KTN Crystals

### introduction

The sensitivity to cooperative processes at the molecular level is one of the many attractive features of Dielectric Spectroscopy. We have applied the techniques of Time Domain Dielectric Spectroscopy (TDS) in order to probe the relaxational dynamics of the Ferroelectric Phase Transition in  $\text{KTa}_{1-x}\text{Nb}_x\text{O}_3$  (KTN) crystals [1]. The results were able to expose the percolative nature of the phase transition in these crystals and monitor the behaviour of the dipolar entities interacting within.

KTN is a member of the  $\text{ABO}_3$  perovskite family and has attracted great interest both as a model system and for its optical properties [2]. The Nb ion sitting in the central lattice site (B) has been shown to reside slightly off-center forming dipolar entities. The presence of these off-centred ions is significant because they can begin to form nanoregions with relaxational behaviors correlated over mesoscopic length scales [3].

The KTN crystal used in the current investigation was grown using the top seeded solution growth method and the Ta/Nb ratio was estimated by electron microprobe analysis to be approximately 62/38 per mole. A sample of  $1 \times 1 \times 2 \text{ mm}^3$  was cut from the grown boule along the crystallographic [001] axes. The x-y faces of the sample (perpendicular to the growth direction z) were polished and coated with gold electrodes.

The dielectric measurements were performed using the TDS-2 (Dipole) set-up [2] consisting of a signal recorder, a sampler and a built-in pulse generator. The generator produced 200 mV pulses of 10  $\mu\text{s}$  duration and short rise time  $\sim 30 \text{ ps}$ . The sampler channel was characterized by an 18 GHz bandwidth and 1.5 mV noise (RMS). The form of the measured voltage pulse and the response of the sample were digitized and averaged by the digitizing block of the Time Domain Measurement System. The sample cell was an ordinary plate capacitor terminated to the central electrode on the end of the coaxial line and its temperature was controlled by a Julabo F10 circulatory heat bath.

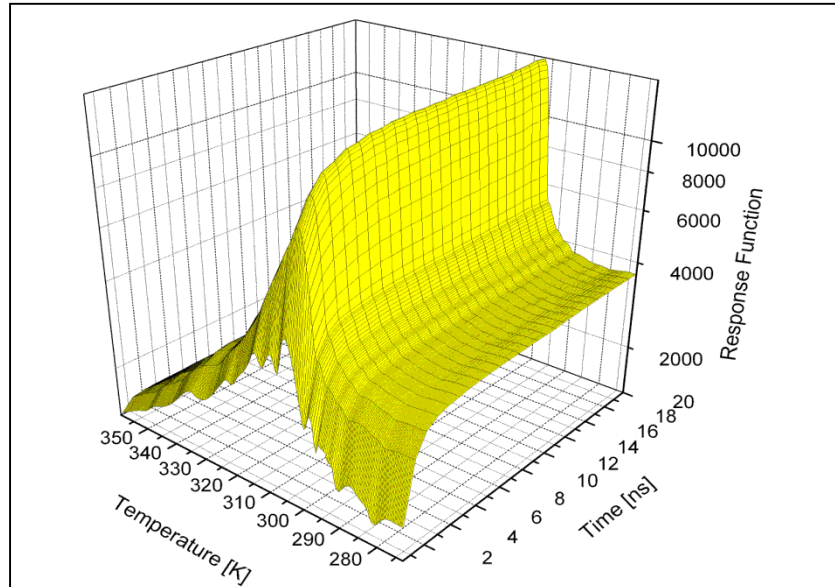


Fig. 1a. 3-D plot of Response function with both time and temperature dependence.

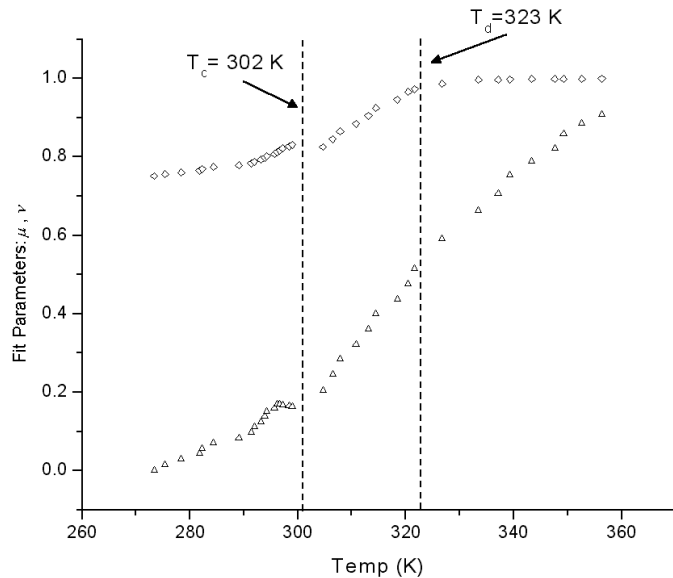


Fig. 1b. Temperature dependence of the fitting parameters  $\nu(\diamond)$  and  $\mu(\Delta)$  obtained from the fit. The percolation onset ( $T_d=323\text{K}$ ) and the Ferroelectric transition ( $T_c=302\text{K}$ ) are clearly noted in their behaviour.

Temperature range of the TDS measurements was from 270-360 K.

### main results and discussion

One advantage of the measurements in the time domain is the ability to extract the dielectric response function  $\Phi(t)$  directly. The convolution integral giving this response takes the form:

$$Q(t) = C_0 \left( \epsilon_\infty V(t) + \int_0^t \dot{\Phi}(t-t') V(t') dt' \right) \quad (1)$$

with  $Q(t)$  the accumulated charge,  $V(t)$  the applied voltage, and  $C_0$  the empty cell capacitance. Being that the response  $\Phi(t)$  is associated with the macroscopic dipole correlation function, it therefore contains information directly related to the

structural and kinetic properties of the sample and can be used to characterize the dynamic properties of the system.

The phenomenological function used to fit the data was a product of a stretched exponent and power-law dependencies in the form of:

$$\Phi(t) = \Delta \epsilon \left[ 1 - t^{-\mu} \exp \left\{ - \left( \frac{t}{\tau} \right)^\nu \right\} \right] \quad (2)$$

In this expression  $\tau$  represents the relaxation time and  $\Delta \epsilon$  the dielectric strength of the complex process related to the dipolar entity. The power and stretch parameters  $\mu$  and  $\nu$  shown in Figure 1 are intricately related with the percolation

phenomena and can be interpreted in connection with the recursive fractal model [4].

Within this context the relationship between the phenomenological exponent  $\nu$ , and the underlying fractal dimension  $D_f$  related to the paths of excitation may be derived from proportionality and scaling relations. Assuming that the fractal geometry is isotropic and has spherical symmetry:

$$D_f = d \cdot \nu \quad (3)$$

with  $d$  representing the initial fractal dimension. The behavior of the parameter  $\nu$  in conjunction with relation (3) thus allows the monitoring of this fractal dimension. In our case the excitation is the polarization vector and its evolution determined by the spanning network of the Nb polar clusters. The results indicate that this cluster formation begins at  $T_d$  about 20 degrees above the phase transition. The parameter  $\mu$  on the other hand reflects the independent parallel growth of the correlation length of each dipolar entity, even while there are no mutual interactions. This process is much slower and consequently related to longer time scales. Below  $T_c$  this length diverges and the parameter  $\mu$  is close to zero.

**the role of TDS**

The measurement of these dielectric properties could not have been performed accurately using any technique other than TDS. The value of the permittivity  $\epsilon'$  in ferroelectric crystals (KTN included - Figure 2) is often tens of thousands. The standard high-frequency methods (RF impedance analyzers, etc.) aren't suitable when dealing with such high values of dielectric permittivity. The phase shift at the sample is too high and immediately exceeds  $2\pi$  at every frequency step making accurate measurement extremely difficult. For materials where  $\epsilon'$  is only a few thousand some measurements can be made up to 1 GHz using specially designed sample cells [5].

The TDS method is ideally suited to circumvent these experimental errors. The accuracy of the time domain measurements is determined primarily by the signal-to-noise ratio. Typical systems may have error values of up to 5%. In this case the phase shift in frequency domain actually works to our advantage. It corresponds in the time domain to a time shift thus increasing the signal accuracy by reducing the errors coming from the time shift between

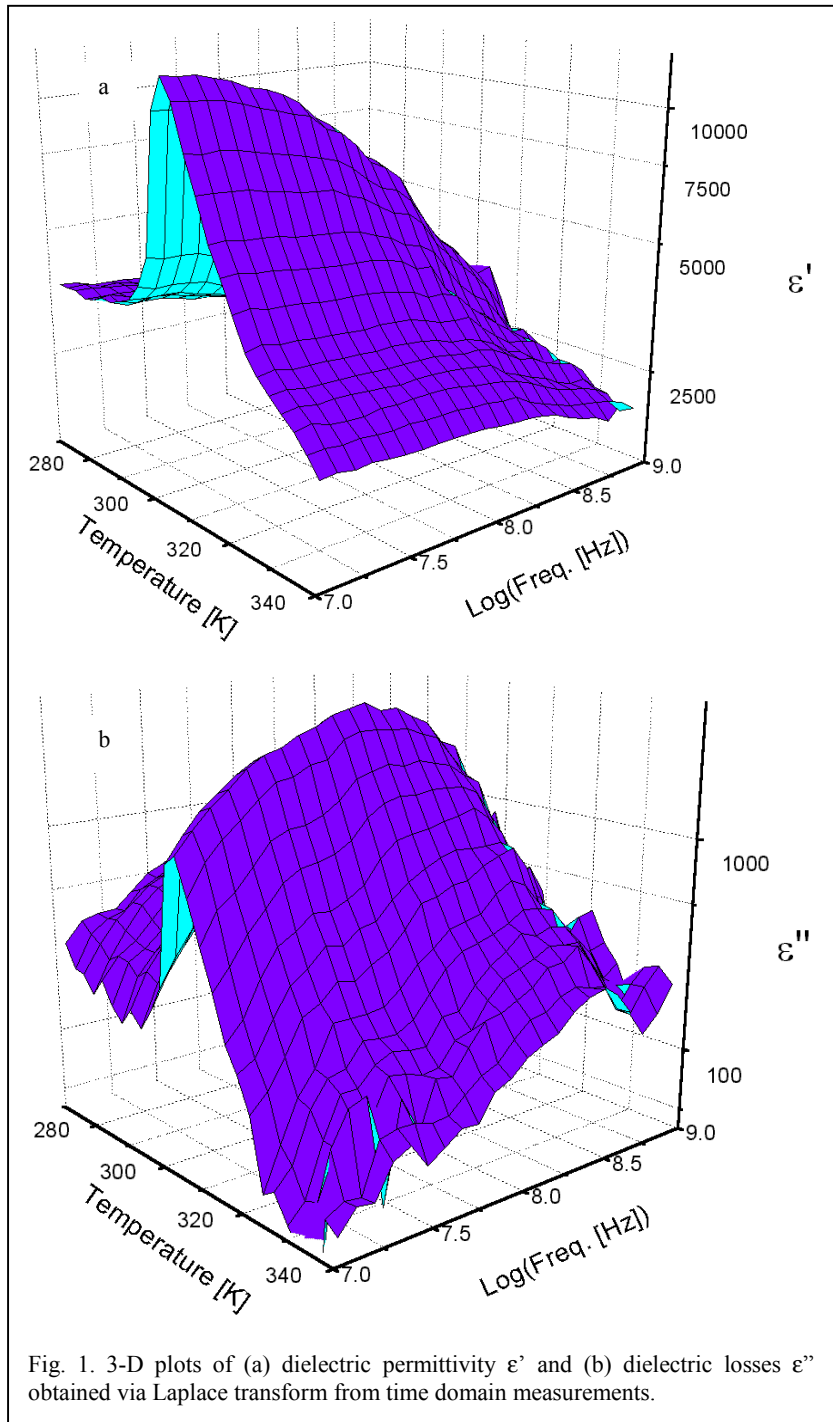


Fig. 1. 3-D plots of (a) dielectric permittivity  $\epsilon'$  and (b) dielectric losses  $\epsilon''$  obtained via Laplace transform from time domain measurements.

the signal reflected from the sample and the calibrated reference standard.

The results presented above clearly show that it is possible to utilize the method of TDS to obtain meaningful results on systems with very high dielectric permittivity. The method is capable of supplementing the frequency-based methods in the study of materials that have proven most difficult to study otherwise.

*References*

[1] Lerner S. E.; Ben Ishai P.; Agrant A. J.; Feldman Y. *J. Non.-Crys. Solids*, in press

[2] Feldman Y.; Puzenko A.; Ryabov Y. *Adv. Chem. Phys.* **133A**, 1 (2006)

[3] Samara G. A. *J. Phys: Condens. Matter* **15**, R367 (2003)

[4] Shlesinger M. F.; Zaslavsky G. M.; Klafter J. *Nature* **363**, 31 (1993)

[5] Spectroscopy of Ferroelectrics and Related Materials, Grigas J. Gordon and Breach: Amsterdam (1996)

Shimon E. Lerner, Paul Ben Ishai, and Prof. Yuri Feldman  
Department of Applied Physics, The Hebrew University of Jerusalem, Givat Ram, 91904, Jerusalem, Israel

G. Schaumburg

**Novocontrol Introduces High Quality Low Cost Interdigitated Comb Electrodes**

Novocontrol introduces a new series of high quality interdigitated electrodes (IE). For convenient sample attachment, the comb structures have a round shape with 15 or 20 mm diameter  $D$  as shown in fig. 1.

The spacing between the comb fingers  $s$  and their width  $w$  as shown in fig. 2 are both 150  $\mu\text{m}$ . This results in an empty cell capacity  $C_0$  of the upper half electrode as defined below by (2) of 7 pF for  $D = 20$  mm and 4 pF for  $D = 15$  mm. Customized versions with  $w$  and  $s$  down to 50  $\mu\text{m}$  are available on request.

The electrode combs are made of gold plated copper layers with 35  $\mu\text{m}$  height  $h$ . The copper fingers have a low ohmic resistance in the 10 m $\Omega$  range which allows measurements at frequencies up to 10 MHz and for materials with conductivity from  $10^{-17} \dots 0.1$  S/cm on a single IE.

This is in contrast to comb electrodes created by evaporation or sputter techniques which create metal layers with a thickness in the 100 nm range resulting in comb electrode resistance in the k $\Omega$  range.

The comb structures are located on a silica reinforced high insulating substrate material with loss factor  $\tan(\delta) < 10^{-3}$  in the frequency range from 1 Hz .. 1 MHz at 20 °C and below.

The IE can be used at temperatures from -160 .. 250 °C. For one time applications like e.g. monitoring of cure, special low cost versions are available.

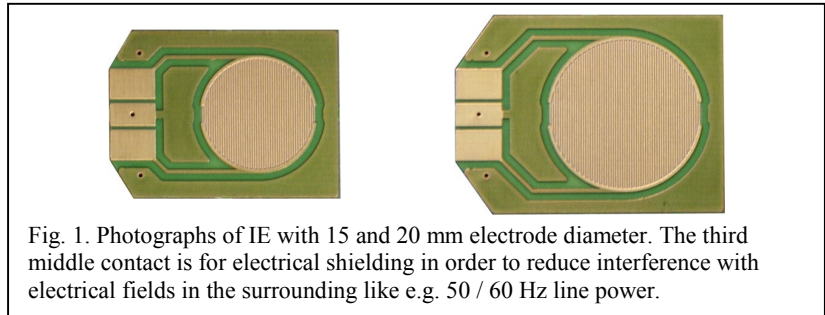


Fig. 1. Photographs of IE with 15 and 20 mm electrode diameter. The third middle contact is for electrical shielding in order to reduce interference with electrical fields in the surrounding like e.g. 50 / 60 Hz line power.

**interdigitated electrodes**

are made up by two overlapping metal comb structures deposited on a substrate as shown in fig. 2a. Each metal comb acts as one electrode. The sample material is deposited on the free opposite site of the substrate and has direct contact to the comb electrodes.

This configuration creates an electric field distribution which is mainly concentrated within a thin layer with thickness  $d$  at the interface between substrate and sample material.  $d$  approximately corresponds to the length of one electrode base cell  $w + s$  as shown in fig. 2b. Therefore IE are mainly sensitive to a surface layer with thickness  $d$  of the sample and substrate material. They are therefore convenient in order to measure the electrical properties of liquids or materials which can be created on IE by e.g. evaporation or spin coating.

The main advantages with respect to parallel plate electrodes are:

- The sample is attached only at one side to the electrode. The other sample side remains free and can be used for additional applications like e.g. optical observations and application of light and gases. This has a wide range of sensor applications where the electrode is covered by a material which changes its electrical properties as a function of a parameter of interest like e.g. the

concentration of a specific gas or pressure.

- As the electrode geometry is fixed for samples with thickness sufficiently exceeding  $d$ , no sample related geometry parameters like sample thickness are required. E.g. in order to measure a liquid, the electrode can be simply immersed or a small amount of liquid can be dropped on the electrode.

On the other hand the following restrictions exist for IE.

- The measured impedance contains contributions from both the sample material and substrate. This can result at significant errors especially for low loss or high insulating samples.

- At higher frequencies or for samples with high conductance or permittivity, the resistance and inductance of the comb electrodes can significantly contribute to the total measured impedance of the IE. These effects are difficult to compensate and limit the usable impedance and frequency range.

**evaluation of permittivity**

In order to evaluate the general complex sample permittivity  $\epsilon_s^*$  and conductivity

$$\sigma_s^* = j\omega\epsilon_0(\epsilon_s^* - 1) \quad (1)$$

from the impedance  $Z_m^*$  measured at the IE contacts, one assumes that the electrical field distribution as shown in fig. 2b on both sides of the comb structure does not depend on the sample and substrate permittivity. This assumption seems to be fulfilled for symmetry reasons if the electrode configuration is exactly symmetrical with respect to the sample to substrate interface plane. In this case, the upper and lower side can be considered as two electrically independent volumes creating two independent capacitors with an total capacity of

$$C_m^* = C_0(\epsilon_s^* + \epsilon_{su}^*) \quad (2).$$

From this the measured impedance follows from

$$Z_m^* = \frac{-j}{\omega C_m^*} \quad (3)$$

where  $C_0$  is the empty cell capacity of both the lower and upper capacitor,

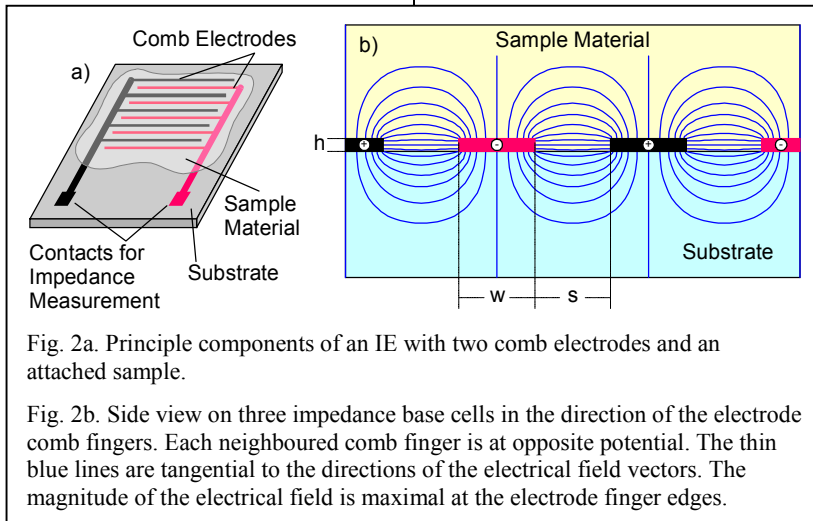


Fig. 2a. Principle components of an IE with two comb electrodes and an attached sample.

Fig. 2b. Side view on three impedance base cells in the direction of the electrode comb fingers. Each neighbored comb finger is at opposite potential. The thin blue lines are tangential to the directions of the electrical field vectors. The magnitude of the electrical field is maximal at the electrode finger edges.

$\epsilon_{su}^*$  substrate permittivity,  $j$  imaginary unit,  $\omega = 2\pi$  frequency and  $\epsilon_0$  vacuum permittivity.

In addition to the two capacitors described by (2), the comb electrodes have a serial impedance  $Z_{co}^*$  due to the ohmic resistance and the inductance of the comb metal. The above equations assume that  $Z_{co}^*$  is low to  $Z_m^*$ . Otherwise, the evaluation becomes complicated as the potential on each electrode and with this the electrical field distribution locally depends on the position on the electrode. As a first order correction,  $Z_{co}^*$  can be added to (3) which results in

$$Z_m^* = Z_{co}^* - \frac{j}{\omega C_m^*} \quad (4).$$

Nevertheless, in practice one usually confines  $Z_m^*$  to an impedance range were  $Z_{co}^*$  can be neglected.

**thin films**

For thin films with thickness  $d_s$  in the same dimension or small against the electrode base cell length  $d = w + s$ , it has to be considered that the volume where the electrical field  $E$  on the IE sample side is concentrated is only partly filled by the sample.

For this purpose, one can assume in first order approximation that the absolute value of  $E$  is constant within a surface layer with thickness  $d$  at the free substrate side and 0 outside. In this case, the IE sample side can be separated into one capacitor created by the thin film and an additional air capacitor with a permittivity of 1 and thickness  $d - d_s$ . In correspondence to (2), this results in a total IE capacity of

$$C_m^* = C_0 \left( \epsilon_s^* \frac{d_s}{d} + 1 \frac{d - d_s}{d} + \epsilon_{su}^* \right) \quad (5)$$

for  $d_s \leq d$ .

**sensitivity**

is defined as e.g. for the real part of  $C_m^*$  as

$$S' = \frac{\text{relative change in } C_m'}{\text{relative change in } \epsilon_s'} \quad (6)$$

For the imaginary part a corresponding definition applies.

$S'$  and  $S''$  are for a parallel plate capacitor = 1. For the IE in the thick sample limit, the sensitivity decreases with the ratios of  $\epsilon_s'/\epsilon_{su}'$  and  $\epsilon_s''/\epsilon_{su}''$ .

E.g. for  $\epsilon_s' = \epsilon_{su}' = 3$ , from (2) follows  $S' = 0.5$ . The situation gets more critical for  $\epsilon_s''$  which for low loss materials gets low. E.g. for  $\epsilon_s'' = 10^{-4}$  and  $\epsilon_{su}'' = 10^{-2}$ ,  $S'' = 0.01$  which means that in this case 100% change in  $\epsilon_s''$  results only in 1% change of  $C_m''$  and with this the IE is nearly insensitive to low  $\epsilon_s''$  values.

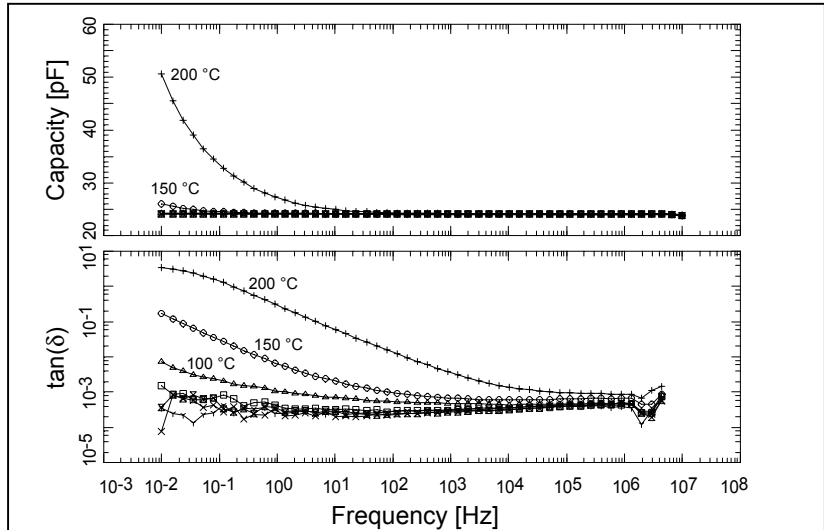


Fig. 3. Measured capacity and loss factor  $\tan(\delta)$  of the empty IE for temperatures from -100 .. 200 °C in 50 °C steps.

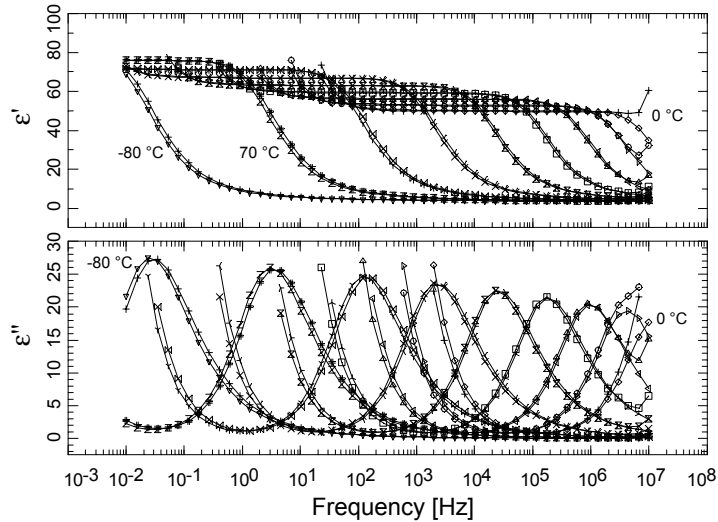


Fig. 4. General permittivity of Glycerol measured both by an IE and a parallel plate capacitor for comparison at temperatures from -80 .. 0 °C in 10 °C steps. The IE lines are slightly shifted to lower frequencies due to temperature gradients within the IE to the sample cell temperature sensor. For high permittivity at the high frequency end, the IE lines both for  $\epsilon'$  and  $\epsilon''$  deviate to higher values due to the  $Z_{co}^*$  contribution.

For the thin film limit  $d_s \ll d$ , according to (5) the IE becomes insensitive to  $\epsilon_s'$  if the ratio  $(\epsilon_s' d_s/d)/(\epsilon_{su}' + 1) \ll 1$  and insensitive to  $\epsilon_s''$  if the ratio  $(\epsilon_s'' d_s/d)/\epsilon_{su}'' \ll 1$ . In order to e.g. measure a 10 nm thick film with  $\epsilon_s' = 4$  with 10%  $\epsilon_s'$  sensitivity, an IE with a base cell length of  $d = 100$  nm would be required. On the other hand, if the film has an  $\epsilon_s''$  of 1500 due to a conductivity contribution from (1), a  $d$  of 150  $\mu\text{m}$  would be sufficient for 10%  $\epsilon_s''$  sensitivity.

**calibration**

In order to evaluate the sample permittivity from (2), (3) and (5), the parameters  $C_0$  and  $\epsilon_{su}^*$  have to be known. They can be easily derived by dividing and subtracting the measured  $C_m^*$  from a calibration

material with known dielectric function and a second empty electrode measurement.

With this, the IE can in principle be completely calibrated. In practice, the situation is more complicated as  $\epsilon_{su}^*$  is both frequency and temperature dependent, which requires corresponding calibration measurements. Even if available, the measured data will only be partly useful as in regions of low sensitivity, the results may be affected by drift which is mainly caused by humidity pickup of the substrate material.

**example measurements**

All data were measured by a Novocontrol Alpha-A analyzer in combination with a ZGS active sample cell and Quatro Cryosystem.

The capacity and loss factor  $\tan(\delta)$

of an empty IE with  $D = 20$  mm is shown in fig. 3 for several temperatures.  $\tan(\delta)$  is below  $10^{-3}$  nearly over the entire frequency range. At temperatures above  $50$  °C  $\tan(\delta)$  increases at lower frequencies due to ion conductivity of the substrate material. This results in a capacity increase at low frequencies due to electrode polarization effects, too.

Fig. 4 shows a comparison of results measured by a reference parallel plate capacitor and an IE with  $D = 20$  mm. Glycerol was chosen for the test material as its dielectric properties have been extensively evaluated e.g. [1], it shows a strong relaxation, and both  $\epsilon'$  and  $\epsilon''$  show strong variations over a wide dynamic range if measured within the relevant frequency and temperature ranges.

The data were evaluated from (2) and (3). For reasons of simplicity,  $\epsilon_{su}^*$  was approximated by a constant real number ( $\epsilon_{su}^* = 2.4$ ). As can be seen from fig. 4, within the limits of experimental error no deviations of the measured data were found.

*References*

[1] Glassy Dynamics, P. Lunkenheimer, U. Schneider, R. Brand, and A. Loidl, Contemporary Physics, **41-1**, 15 (2000)

Dr. G. Schaumburg  
Novocontrol Technologies, Germany

**Book Review**  
**Electrical Properties**  
**of Polymers**

by E. Riande and R. Diaz-Calleja,  
Marcel Dekker, Inc, New York.  
Basel 2004, v-ix and 630 pp.

*Broadband Dielectric Spectroscopy* (BDS) is a fairly mature technique compared with others used to study the dynamics of polymer materials, e.g NMR and quasi-elastic light scattering. It has become increasingly important because of its vast frequency/time range and the advances in dielectric theory, which allow direct analyses of BDS data in terms of molecular relaxation and transport processes. The early text by McCrum, Read & Williams (1967) on the BDS/mechanical relaxations of polymers needed updating to reflect the enormous growth in the BDS literature. This has been partially achieved through the books by Runt

& Fitzgerald (1997), Havriliak & Havriliak (1997) and Kremer & Schönhal's (2003) and is continued with this major new book by leading dielectrics researchers Riande and Diaz-Calleja.

Its main emphasis lies in a thorough up-to-date description of phenomenological and molecular theories of the electrical properties of polymers arising from dipole relaxation and ionic conduction, taken together with representative BDS data. Divided into three parts, Part I starts with two Chapters giving the theories of the electrostatics of dipoles, local electrical fields and of static permittivity of dipolar materials by Debye, Onsager, Fröhlich and Kirkwood; rotational brownian motions, linear response theory, relations for complex permittivity in terms of local field factors, molecular dipole moments and time-correlation functions (*TCFs*) of angular motions of molecules. An advanced treatment of the thermodynamics and irreversible thermodynamics of materials in electric fields is given (Ch.3) and Part I concludes with Ch.4 that summarizes briefly dielectric measuring techniques (A.C., transient response and thermally-stimulated currents) and commonly-used empirical relaxation functions.

Part II (Ch.5) describes the equilibrium statistics of chain molecules, their apparent dipole moments and static permittivity, the E-field-induced birefringence (Kerr-effect) of polymer solutions in static fields (Ch.6) and 'molecular dynamics' simulations for the determination of *TCFs* for the dielectric relaxation of flexible chain polymers in bulk and solution (Ch.7). These are followed by accounts of (i) dielectric relaxation in amorphous materials arising from segmental and long range (normal-mode) motions of chains (Ch.8) and (ii) secondary relaxations in the glassy state, in which the rotation-isomeric model is applied to specific modes of local chain motions (Ch.9). Part II concludes with a brief account of the theory of the dynamic Kerr-effect arising from rotational diffusion (Ch.10).

Part III starts with a description of the molecular structures and organisations in liquid crystals (LC) and theories of the static and complex permittivities of LC and LC polymers, illustrated with experimental results for nematic, smectic and ferroelectric materials in

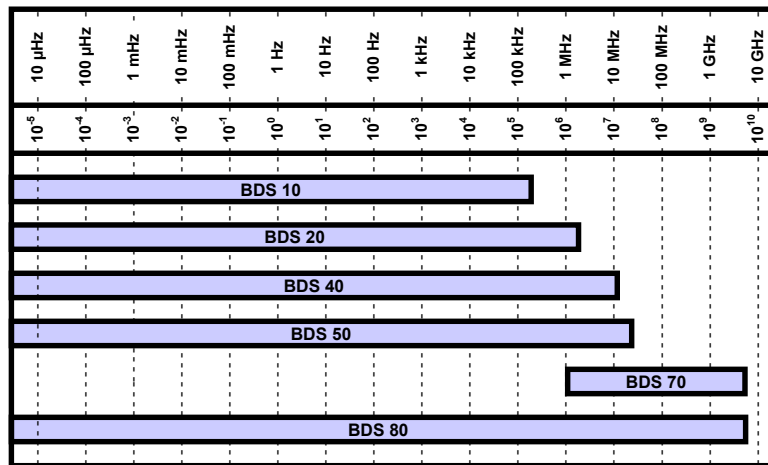
unaligned and aligned states (Ch.11). Piezoelectric and pyroelectric polymers are described in Ch.12, with full theory given for the dielectric tensors involved taken together with representative data for different materials. Ch.13 describes the theory and practice of the non-linear dielectric permittivity of polymers, especially in relation to optical harmonic-generation and rectification, molecular aspects of E-field poling and decay of electroactive function. Finally Ch.14 surveys briefly the theory and practice of semi-conduction in conjugated polymers such as doped polyacetylene, polypyrrole and polyaniline.

The book gives a valuable up-to-date account of the dielectric properties of polymers arising from molecular relaxation processes. The technical production of text, equations and figures is excellent and it reads well. Little attention is given to ionic-conduction behaviour, as in polyelectrolytes, but that would have greatly extended the book. Most Chapters conclude with a Problems Section so, in addition to being a research text, it has a valuable teaching function for advanced students. The authors emphasise throughout how different macroscopic dielectric phenomena are directly-related to chain structure and chain dynamics and, in the case of LC polymers, the macroscopic ordering of the phase. This 'molecular approach' is to be welcomed in dielectrics science since it advances our understanding beyond that achievable using phenomenological theories of dielectric phenomena. It was not possible to give comprehensive accounts of the large experimental BDS literature for each of the topics covered in the book, but many examples are given that illustrate representative behaviour and lead a reader to that larger literature. The authors are to be congratulated on the production of this fine, important book.

Prof. G. Williams, Department of Chemistry, University of Wales Swansea, SWANSEA SA2 8PP, UK.  
g.d.williams@keele.ac.uk

## OVERVIEW

### BROADBAND DIELECTRIC AND IMPEDANCE SPECTROSCOPY over 16 decades by Novocontrol Technologies



## Factory and Head Office

### NOVOCONTROL TECHNOLOGIES GmbH & Co. KG

#### Germany

Obererbacher Straße 9  
D-56414 Hundsangen / GERMANY  
Phone: ++49 64 35 - 96 23-0  
Fax: ++49 64 35 - 96 23-33  
Mail: [novo@novocontrol.de](mailto:novo@novocontrol.de)  
Web: [www.novocontrol.de](http://www.novocontrol.de)

Contact: Dr. G. Schaumburg

#### United Kingdom

Additional Technical and Sales Support for British Customers  
Headways, Shoulton, Hallow,  
Worcester WR2 6PX / United Kingdom  
Phone: ++(0) 870 085 0744  
Fax: ++(0) 870 085 0745  
Mail: [jed@novocontrol.de](mailto:jed@novocontrol.de)

Contact: Mr. Jed Marson ++(0) 7974 926 166

## Agents

#### USA/Canada

NOVOCONTROL America, Inc.  
8537 Purnell Ridge Road  
Wake Forest, NC 27587  
USA  
Phone: +1 919 554 9904 Toll free: +1-866 554 9904  
Fax: +1 919 556 9992  
Mail: [novocontrolusa@earthlink.net](mailto:novocontrolusa@earthlink.net)  
Contact: Mr. Joachim Vinson, PhD

#### Japan

Morimura Bros. Inc.  
2 nd chemical division  
Morimura Bldg. 3-1, Toranomon 1-chome  
Minato-Ku, Tokyo 105 / Japan  
Phone: ++(0) 3-3502-6440  
Fax: ++(0) 3-3502-6437  
Mail: [hasegawa@morimura.co.jp](mailto:hasegawa@morimura.co.jp)  
Contact: Mr. Hasegawa

#### Greece

Vector Technologies Ltd.  
40 Diogenous Str. 152  
34 Halandri, Athens  
Phone: (0030) 210 6858 008  
Fax: (0030) 210 6858 118  
Mail: [info@vectortechnologies.gr](mailto:info@vectortechnologies.gr)  
contact: Mr. Vouvous

#### People's Rep. Of China

GermanTech Co. Ltd  
Room 706, No. 7 Building, Hua Qing Jia Yuan  
Wu Dao Kou, Haidian District  
Beijing, 100083 / China  
Phone: ++(10) 82867920/21/22  
Fax: ++(10) 82867919  
Mail: [contact@germantech.com.cn](mailto:contact@germantech.com.cn)  
[xysun@germantech.com.cn](mailto:xysun@germantech.com.cn)  
Contact: Mr. Xiaoyu Sun

#### Taiwan

JIEHAN Technology Corporation  
No. 58, Chung Tai East Road, 404  
Taichung / Taiwan  
Phone: ++886-4-2208-2450  
Fax: ++886-4-2208-0010  
Mail: [jiehantw@ms76.hinet.net](mailto:jiehantw@ms76.hinet.net)  
Contact: Mr. Peter Chen

#### South Korea

PST Polymer Science Technologies  
Rm. 716, Hojung Tower, 528-13  
Anyang-shi, Kyungki-Do, Korea  
Phone: 031-507-8552  
Fax: 031-448-6189  
Mail: [sunpoint@hanafos.com](mailto:sunpoint@hanafos.com)  
Contact: Mr. Young Hong

#### Middle East

National Scientific Company Ltd.  
P.O.Box 437  
Riyadh 11411 K.S.A.  
Phone: +966 1 473 6284  
Fax: +966 1 473 7759  
Mail: [nsc@diginet.sa](mailto:nsc@diginet.sa)  
Contact: Mr. Osama Ali

Editor Dielectrics Newsletter: Gerhard Schaumburg. Abstracts and papers are always welcome. Please send your script to the editor